Deletion of CD226 in Foxp3^{+} T cells Reduces Diabetes Incidence in Non-Obese Diabetic Mice by Improving Regulatory T Cell Stability and Function

Puchong Thirawatananond[1], Matthew E. Brown[1], Lindsey K. Sachs[1], Juan M. Arnoletti[1], Wen-I Yeh[1], Amanda L. Posgai[1], Melanie R. Shapiro[1], Yi-Guang Chen[2], Todd M. Brusko[1,3]

[1]Department of Pathology, Immunology and Laboratory Medicine, College of Medicine, Diabetes Institute, University of Florida, Gainesville, FL 32610

[2]Department of Pediatrics, Medical College of Wisconsin, Milwaukee, WI 53226

[3]Department of Pediatrics, College of Medicine, Diabetes Institute, University of Florida, Gainesville, FL 32610

Correspondence to: Todd Brusko, PhD, Department of Pathology, Immunology and Laboratory Medicine, College of Medicine, University of Florida, 1275 Center Drive, Biomedical Sciences Building J-589, Box 100275, Gainesville, FL 32610. E-mail address: tbrusko@ufl.edu. TEL: (352) 273-9255. FAX: (352) 273-9339. ORCID ID: 0000-0003-2878-9296

Word Count: 5292

Abstract: 246

Figures: 6

Supplementary Figures: 7

22 **Abstract**

23 Co-stimulation serves as a critical checkpoint for T cell development and activation, and several
24 genetic variants affecting co-stimulatory pathways confer risk for autoimmune diseases. A single
25 nucleotide polymorphism in *CD226* (*rs763361*; G307S) has been shown to increase susceptibility
26 to type 1 diabetes, multiple sclerosis, and rheumatoid arthritis. CD226 competes with the co-
27 inhibitory receptor TIGIT (T cell immunoreceptor with Ig and ITIM domains) to bind CD155 to
28 amplify TCR signaling. We previously found that *Cd226* knockout protected non-obese diabetic
29 (NOD) mice from disease, but the impact of CD226 signaling on individual immune subsets
30 remained unclear. We focused on regulatory T cells (Tregs) as a population of interest, as prior
31 reports demonstrated that human CD226^{+} Tregs exhibit reduced FOXP3^{+}Helios^{+} purity and
32 suppressive function following expansion. Hence, we hypothesized that global deletion of *Cd226*
33 would increase Treg stability and accordingly, Treg-specific *Cd226* deletion would inhibit diabetes
34 in NOD mice. Indeed, crossing the NOD.*Cd226*$^{-/-}$ and NOD.*Foxp3*-GFP-Cre.*R26*-loxP-STOP-
35 loxP-YFP Treg-fate tracking strains resulted in increased Treg induction and decreased FoxP3-
36 deficient "ex-Tregs" in the pancreatic lymph nodes. We generated a Treg-conditional knockout
37 (Treg$^{\Delta Cd226}$) strain and found that female Treg$^{\Delta Cd226}$ mice had decreased insulitis and diabetes
38 incidence compared to Treg^{WT} mice. Additionally, we observed increased TIGIT expression on
39 Tregs and conventional CD4^{+} T cells within the pancreas of Treg$^{\Delta Cd226}$ versus Treg^{WT} mice. These
40 findings demonstrate that an imbalance of CD226/TIGIT signaling may contribute to Treg
41 destabilization in the NOD mouse and highlight the potential for therapeutic targeting of this
42 pathway to prevent or reverse autoimmunity.

43 **Introduction**

44 Co-stimulatory signaling is essential for the development and activation of T lymphocytes, and
45 gene variants converging on several co-stimulatory pathways confer risk for autoimmune diseases,
46 including type 1 diabetes (T1D). The *rs763361* (C>T) single nucleotide polymorphism (SNP)
47 within the *CD226* gene, for example, has been shown to increase susceptibility to T1D, multiple
48 sclerosis (MS), and rheumatoid arthritis (RA) (1, 2). CD226, also known as DNAX accessory
49 molecule-1 (DNAM-1), is expressed on natural killer (NK) cells (3), $CD8^+$ T cells (4), platelets
50 (5), monocytes (6, 7), and activated $CD4^+$ T cells (8). CD226 competes with the co-inhibitory
51 receptors TIGIT (T cell immunoreceptor with Ig and ITIM domains) and CD96 to bind the ligand
52 CD155 (poliovirus receptor, PVR) on antigen presenting cells (APCs) (9). Upon ligation, CD226
53 initiates phosphorylation of its cytoplasmic tail leading to downstream PI3K/Akt and MAPK/Erk
54 signaling, and inducing T cell activation and proliferation (3). The autoimmune-associated Ser^{307}
55 variant, encoded by the *rs763361* (T) allele, is thought to potentially provide an additional
56 cytoplasmic phosphorylation site, augmenting downstream signaling (10). Hence, there is a need
57 to understand how CD226 activity may contribute to the pathogenesis of T1D and other
58 autoimmune diseases.

59 $CD4^+$ regulatory T cells (Treg) play an important role in T1D, with the majority of T1D
60 immunotherapies seeking to augment Treg function or frequency relative to effector T cell subsets
61 (11, 12). We previously reported that IFN-γ producing Tregs were enriched in CD226 expression
62 (13). However, how CD226 signaling affects Treg stability and function during T1D development
63 remains unclear. We previously reported that expanded human $CD226^+$ Tregs had increased
64 expression of interferon-γ as well as decreased suppression of $CD4^+$ and $CD8^+$ T cell responders
65 compared to $CD226^-$ Tregs (14). Building on this, we observed increased $FOXP3^+Helios^+$ purity

66 and *in vitro* suppressive capacity in $CD4^+CD25^+CD226^-$ versus $CD4^+CD25^+CD127^{lo/-}$ sorted
67 Tregs, supporting the potential utility of CD226 as a negative selection marker for improved
68 sorting prior to Treg adoptive cell therapy (15). Consistent with these observations, Sato et al.
69 recently identified CD226 signaling as a potential source of Treg instability, finding that pre-
70 treatment of human peripheral blood mononuclear cells (PBMCs) with an α-human CD226
71 blocking antibody diminished graft versus host disease (GvHD) development in a humanized
72 mouse model by increasing human $CD4^+FOXP3^+$ Treg numbers and upregulating their FOXP3
73 expression (16).

74 We previously investigated the causal role of CD226 signaling in autoimmune diabetes
75 through the genomic knockout (gKO) of *Cd226* in the non-obese diabetic (NOD) mouse model of
76 T1D (17). Genetic deletion of *Cd226* led to reduced diabetes incidence and insulitis severity.
77 Additionally, this germline deletion was associated with increased $CD8^+$ T cell output from the
78 thymus but decreased $CD44^+CD62L^-$ memory $CD8^+$ T cells in the pancreatic lymph nodes (PLN)
79 and islet-specific glucose-6-phosphatase catalytic subunit related protein (IGRP)-specific memory
80 $CD8^+$ T cells in the pancreas. Despite our findings suggesting that *Cd226* gKO primarily impacted
81 the pathogenicity of $CD8^+$ T cells, adoptive transfer of mixed populations of *Cd226*$^{+/+}$ and *Cd226*$^-$
82 $^{/-}$ T cells into immunodeficient NOD.*scid* recipients demonstrated a requirement for CD226 on
83 $CD4^+$ T cells to confer disease (17). In line with our findings, Wang and colleagues demonstrated
84 that CD226 gKO delayed disease onset in the experimental autoimmune encephalomyelitis (EAE)
85 mouse model of MS (18). Interestingly, *Cd226*$^{-/-}$ EAE mice also had increased amounts of Tregs
86 and increased induced Treg (iTreg) proliferation *in vitro* (18), and α-CD226 blocking antibodies
87 reduced Th1-mediated autoimmunity (8) and increased IL-10 production (19) in the EAE mouse.
88 While these observations collectively support the role of CD226 in promoting the loss of T cell

89 tolerance in NOD and EAE mice, it was unclear whether the influence of CD226 on Treg
90 proliferation and stability would extend to the NOD mouse model.

91 The current study investigates how CD226 signaling impacts Treg frequency and function
92 in the context of the NOD mouse model. We hypothesized that Treg-selective *Cd226* KO would
93 improve Treg stability, resulting in reduced diabetes incidence in these mice. To test this, we
94 generated two novel NOD strains, specifically a Treg-fate reporter (20) *Cd226* gKO and a Treg
95 *Cd226* conditional KO (cKO) strain, for detailed interrogation of Treg-specific contributions
96 toward insulitis and autoimmune diabetes.

97 **Materials and Methods**

98 **Animal Husbandry and Regulatory Approval**

99 Animals were bred and housed in specific-pathogen free facilities at the University of Florida with
100 *ad libitum* access to food and water. Studies were performed with protocols approved by the
101 University of Florida Institutional Animal Care and Use Committee (UF IACUC) and in
102 accordance with the National Institutes of Health Guide for Care and Use of Animals.

103

104 **Mouse Strains**

105 NOD.*Foxp3*-GFP-Cre.*R26*-loxP-STOP-loxP-YFP Treg-fate tracking mice (20) were crossed with
106 our previously reported NOD.*Cd226*$^{-/-}$ (17) strain to generate Treg-fate reporter mice with *Cd226*
107 gKO on the NOD background. The *Cd226* cKO allele was generated at Jackson Laboratories
108 through CRISPR/Cas9-mediated knock-in of loxP within intronic regions flanking exon 2 of the
109 *Cd226* gene on the NOD background. The following single guide RNAs were used: intron 1,
110 GCTATCGTACAGGGATGGAT and GCTTTGCTATCGTACAGGGA; intron 2,
111 TGACATGTGCAGGATCTCTT and GAAATACTAAAATTTACAAG. Founder cKO mice with
112 confirmed loxP knock-ins were backcrossed with NOD mice for one generation before crossing
113 with NOD.*Foxp3*-GFP-Cre mice purchased from Jackson laboratories (20). *Cd226*$^{fl/+}$.*Foxp3*$^{Cre/+}$ x
114 *Cd226*$^{fl/+}$.*Foxp3*$^{+/+}$ breeder pairs were created and, subsequently, *Cd226* Treg-specific cKO (i.e.,
115 *Cd226*$^{fl/fl}$ x *Cd226*$^{fl/fl}$) and *Cd226* intact (*Cd226*$^{+/+}$ x *Cd226*$^{+/+}$) breeding schemes were utilized to
116 obtain Treg$^{\Delta Cd226}$ and Treg^{WT} mice for experiments.

117

118 **Genotyping**

119 The *Cd226* gKO allele genotyping was performed with a custom Taqman SNP assay (Thermo
120 Fisher Scientific) using the following primers: forward, GGGAGCATGAAGAGCATCCT;
121 reverse, GCGACATCTGTAAAGTCCTGAGT; *Cd226* WT reporter (VIC),
122 CAAATGCCATGGCCGCT; *Cd226* gKO reporter (FAM), CAAATGCCATGCCGCT (17). The
123 *Foxp3*-GFP-Cre transgene was genotyped using a SYBR Green PCR Master Mix (Thermo Fisher
124 Scientific) to amplify the GFP allele (forward, GACCCTGAAGTTCATCTGCACC; reverse,
125 CGGGTCTTGTAGTTGCCGTC) and internal control (IC; forward,
126 GGCAAAGGTGGAAATGAAGA; reverse, CTCAGACCACACAGGGAATG). A Roche
127 LightCycler 480 was used to detect GFP and IC amplicons at melting points of 86ºC and 79ºC,
128 respectively. The *Cd226 fl* allele was genotyped using high resolution melting by amplifying with
129 SYBR Green PCR Master Mix (Thermo Fisher Scientific; forward,
130 CTGGCACAGAGGACACACTC; reverse, GCACAGGAAAGAAGTTTCAGC) on a Roche
131 LightCycler 480. Samples were assessed based on melting profiles and difference plots for *Cd226*
132 *fl* (approximately 200 base pairs) versus *Cd226* WT alleles (approximately 180 base pairs).
133

134 **DNA confirmation of Treg *Cd226* cKO**

135 Splenocytes from mice were stained with α-CD4 (PerCP-Cy5.5; clone GK1.5; BioLegend) and α-
136 CD8α (BV711; 53-6.7; BioLegend) and $CD8^+$ T cells, $CD4^+GFP^-$ Tconv and $CD4^+GFP^+$ Treg
137 were sorted on a FACSAria III (BD Biosciences). Sorted cells were then processed with a DNeasy
138 kit (Qiagen), and 2 ng of DNA was amplified with the following primers complementary to *Cd226*
139 gene sequences flanking exon 2: forward: TTGTTGCACAGAGCTAAGTCTG, reverse:
140 CCACCTGGGTTAAGTTATGCG. Samples were then run on a 1.5% agarose (w/v) gel with a
141 100-base pair ladder (Thermo Fisher Scientific).

142

143 **Flow Cytometry**

144 12-week-old euglycemic *Cd226* WT, gKO, Treg$^{\Delta Cd226}$, and Treg^{WT} mice were humanely
145 euthanized, and thymus, spleen, MLN, PLN, and pancreas were harvested. Thymus and spleens
146 were homogenized using a syringe plunger over a 40 µm filter while PLNs were homogenized
147 using two frosted glass microscope slides. Pancreas tissues were minced into 1 mm pieces and
148 incubated in complete RPMI [cRPMI; 50 µg/mL penicillin/streptomycin, 2 mM Glutamax (Life
149 Technologies), 20 mM sodium pyruvate (Gibco), 5 mM non-essential amino acids (Gibco), 5 mM
150 HEPES (Gibco), 10% fetal bovine serum (Biofluid), 20 mM NaOH (Sigma-Aldrich), 50 mM 2-
151 mercaptoethanol (Sigma Aldrich)] with 1 mg/mL collagenase IV (Gibco) and 1 U/mL DNase I
152 (Thermo Scientific) for 18 minutes at 37˚C. Following digestion, pancreas single-cell suspensions
153 were washed with cRPMI and strained through a 40 µm filter. Cells were stained with Live/Dead
154 Near-Infrared dye (L/D NIR; Invitrogen) according to the manufacturer's instructions, then
155 washed with stain buffer. Cells were resuspended in Brilliant Violet Stain Buffer Plus (BD
156 Biosciences) with anti-CD16/32 Fc-Block (BioLegend), then stained with the following antibodies
157 for 30 minutes at room temperature: α-CD3ε (BV605; clone 17A2; BioLegend), α-CD4 (PerCP-
158 Cy5.5; GK1.5; BioLegend), α-CD8α (BV711; 53-6.7; BioLegend), α-CD44 (PE; IM7;
159 BioLegend), α-CD62L (APC; MEL-14; BioLegend), α-CD226 (BV650; TX42.1; BioLegend), α-
160 TIGIT (PE-Dazzle594; 1G9; BioLegend), and α-CD183 (PE-Cy7; CXCR3-173; BioLegend).
161 Cells were washed with stain buffer, then fixed and permeabilized with the eBioscience FOXP3
162 Transcription Factor Staining kit (Invitrogen) according to the manufacturer's instructions. Cells
163 were then stained with α-T-bet (BV421; 4B10; BioLegend) overnight prior to acquisition on a
164 Cytek Aurora 5-laser spectral flow cytometer. The flow cytometric panel assessing thymic Treg

165 frequency included α-CD4 (PerCP-Cy5.5; GK1.5; BioLegend), α-CD8α (BV711; 53-6.7;
166 BioLegend), α-CD44 (PE; IM7; BioLegend), α-CD226 (BV650; TX42.1; BioLegend), and α-Nrp1
167 (BV421; 3E12; BioLegend). The intracellular flow cytometry panel to quantify Treg frequency
168 included α-CD4 (PerCP-Cy5.5; GK1.5; BioLegend), α-CD8α (BV711; 53-6.7; BioLegend), α-
169 CD44 (PE; IM7; BioLegend), α-CD226 (BV650; TX42.1; BioLegend), and α-Helios (Pacific
170 Blue; 22F6; BioLegend). Data were analyzed using FlowJo v10 software (TreeStar).
171

172 **Insulitis and Dacryoadenitis Scoring**

173 Pancreata from Treg$^{\Delta Cd226}$ and Treg^{WT} mice were fixed overnight in 10% formalin in PBS, then
174 washed twice with PBS and stored in 70% ethanol until further processing. Fixed pancreata were
175 paraffin embedded, sectioned at 250 μm steps, stained with hematoxylin and eosin (H&E), and
176 imaged with an Aperio Scancope CS slide scanner. Three sections of pancreas per mouse were
177 scored (mean of islets per mouse: 59.7, standard deviation: 12.4) for insulitis severity by a blinded
178 observer according to previously published criteria (36). Briefly, a score of 0 indicates no
179 infiltration, 1 indicates peri-insulitis, 2 indicates <50% islet immune infiltration, and 3 indicates
180 >50% islet immune infiltration (36). Lacrimal gland inflammatory scoring was performed by
181 quantifying foci (i.e., ≥50 mononuclear cells) and normalizing to 4mm^2 glandular surface area as
182 previously described (37).
183

184 **Diabetes Incidence Study**

185 Blood glucose measurements from Treg$^{\Delta Cd226}$, Treg^{WT} and NOD.*Cd226*$^{fl/fl}$.*Foxp3*$^{+/+}$ mice were
186 taken weekly beginning at 7 weeks of age by collecting a small drop of blood (<5μL) onto an
187 AlphaTRAK 2 glucometer via tail vein prick. Animals registering blood glucose >250 mg/dL had

188 a confirmatory screening 24 hours later, and two consecutive readings >250 mg/dL indicated the
189 onset of diabetes. Mice were monitored until diabetes onset or up to 30 weeks of age, at which
190 time they were humanely euthanized.
191
192 **Phosflow**
193 Splenocytes from Treg$^{\Delta Cd226}$ and Treg^{WT} mice were plated in a 96-well plate at a concentration of
194 1,000,000 cells/mL with plate-bound α-CD3ε (2 μg/mL) and plate-bound CD155 (1 μg/mL;
195 BioLegend) for 15 or 30 minutes at 37ºC. Stimulations were halted with BD Cytofix Fixation
196 Buffer (BD Biosciences) followed by a 10-minute incubation at 37ºC and wash with PBS. Cells
197 were then stained with L/D NIR for 15 minutes and quenched with stain buffer. Fixed cells were
198 permeabilized with 90% methanol for 1 hour and washed with stain buffer twice. Permeabilized
199 cells were incubated with anti-CD16/32 Fc-Block (BioLegend) and stained for CD4 (PerCP-
200 Cy5.5; GK1.5; BioLegend), CD8α (BV711; 53-6.7; BioLegend), p-S6 (PE; D57.2.2E; Cell
201 Signaling Technology), and pAkt (AF647; 193H12; Cell Signaling Technology) overnight at 4ºC.
202 Samples were then acquired on a Cytek Aurora 5-laser spectral flow cytometer, and data were
203 analyzed using FlowJo v10 software (TreeStar).
204
205 ***In Vitro* Proliferation Assay**
206 Splenocytes from Treg$^{\Delta Cd226}$ and Treg^{WT} mice were stained with CellTrace Violet proliferation dye
207 (CTV; Invitrogen) and quenched with cold cRPMI as per manufacturer instructions. Cells were
208 plated in a 24-well plate at a concentration of 500,000 cells/mL on either plate-bound α-CD3ε (2
209 μg/mL; 145-2C11; BioLegend) and soluble α-CD28 (1 μg/mL; 37.51; BioLegend) or plate-bound
210 α-CD3ε (2 μg/mL) and plate-bound CD155-Fc (1 μg/mL; BioLegend) for four days. Cells were

211 then harvested, incubated with anti-CD16/32 Fc-Block (BioLegend), and stained with L/D NIR,
212 α-CD4 (PerCP-Cy5.5; GK1.5; BioLegend), and α-CD8α (BV711; 53-6.7; BioLegend) as
213 described above and acquired on a Cytek Aurora 5-laser spectral flow cytometer. Data were
214 analyzed using FlowJo v10 software (TreeStar).
215
216 **Statistical Analyses**
217 Statistical analysis was performed with GraphPad Prism version 9 (GraphPad Software). Flow
218 cytometry data were analyzed using multiple t-tests with Sidak-Bonferroni multiple comparisons
219 correction, 1-way ANOVA with Bonferroni's multiple comparisons test, and 2-way ANOVA with
220 Sidak multiple comparisons correction. Insulitis scoring was compared by Chi-square test.
221 Diabetes incidence curves were compared by Log-rank (Mantel-Cox) test. P values < 0.05 were
222 considered significant.

223 **Results**

224 **CD226 is upregulated on ex-Treg and effector/memory Treg subsets**

225 Previous studies have shown that expression of CD226 on murine conventional $CD4^+$ T cells
226 (Tconv) is upregulated during initial T cell receptor (TCR) activation and maintained following
227 Th1 skewing (8). We hypothesized that CD226 would be similarly upregulated in activated
228 effector Tregs. Indeed, our analysis of previously published human RNA-seq datasets (21)
229 revealed that *CD226* transcription was increased in activated Tregs compared to resting Tregs (22).
230 To confirm that this observation extended to protein expression levels in mice, we performed flow
231 cytometry to assess CD226 levels on splenocytes from the Treg-fate tracking NOD strain,
232 NOD.*Foxp3*-GFP-Cre.*R26*-loxP-STOP-loxP-YFP. In this strain, Tregs express a GFP-Cre
233 recombinase product driven by a *Foxp3* promoter-driven transgene, which facilitates the
234 permanent expression of YFP under the constitutively active *Rosa26* promoter after excision of a
235 floxed stop codon preceding the YFP transgene. This would provide the ability to discern
236 GFP^+YFP^- "early" Tregs which are thought to be Tregs that recently induced Foxp3 expression,
237 GFP^+YFP^+ stable Tregs, and GFP^-YFP^+ ex-Tregs that have lost Foxp3 expression. The
238 investigators that developed this strain found that ex-Tregs were enriched for a $CD44^+CD62L^-$
239 effector-memory (EM) phenotype and led to hyperglycemia and pancreatic islet destruction during
240 adoptive transfers into NOD *Rag2*$^{-/-}$ recipients (20); hence, we predicted that ex-Tregs would have
241 upregulated CD226 levels compared to "early" Tregs and stable Tregs. As expected, CD226
242 surface expression was increased in the ex-Treg compartment compared to that of early Tregs (1.4-
243 fold; p=0.0289), $CD44^-CD62L^+$ naïve Tregs (2.6-fold; p<0.0001), and $CD44^+CD62L^-$ EM Tregs
244 (1.4-fold; p<0.0001) (**Figure 1A-B** & **Supplemental Figure 1**). In contrast, surface expression of
245 TIGIT was increased in ex-Tregs compared to early Tregs (1.5-fold; p=0.0194) and naïve Tregs

246 (1.4-fold; p<0.0001), but was comparable to EM Tregs (p=0.1576) (**Figure 1C-D**). In addition to
247 the studies demonstrating the role of CD226 in disrupting FOXP3 expression (16) while TIGIT
248 restores Treg suppression (23), this data suggests that an imbalance of CD226:TIGIT signaling
249 might play a role in ex-Treg development, contributing to the loss of Foxp3 expression in EM
250 Tregs and promoting the proliferation of ex-Tregs.
251

252 ***Cd226* gKO reduced ex-Treg frequency in pancreatic lymph nodes of NOD mice**

253 To determine the impact of *Cd226* KO on Treg stability in the NOD mouse, we crossed our
254 NOD.*Cd226* gKO strain (17) with Treg-fate tracking mice and assessed Treg frequencies in
255 various tissues from 12-week-old euglycemic *Cd226*$^{+/+}$ wild-type (WT) and *Cd226*$^{-/-}$ gKO
256 offspring through flow cytometry. Interestingly, frequencies of early (GFP^{+}YFP^{-}), normal
257 (GFP^{+}YFP^{+}), and ex-Tregs (GFP^{-}YFP^{+}) were not significantly altered between *Cd226* WT and
258 *gKO* mice in the thymus, spleen, and mesenteric lymph nodes (**Figure 2A-C**). This suggests that
259 germline loss of CD226 signaling did not impair thymic Treg output to peripheral organs.
260 However, the PLNs of *Cd226* gKO mice had increased early Treg frequencies (9.7-fold; p=0.0002)
261 but decreased normal Treg (0.37-fold; p=0.0016) and ex-Tregs (0.45-fold; p=0.0011) compared to
262 those of *Cd226* WT mice (**Figure 2A-D**). This suggests that CD226 signaling might restrain Foxp3
263 induction while promoting Foxp3 instability in the context of an inflammatory microenvironment
264 such as the PLN in NOD mice. Based on the opposing roles of CD226 and TIGIT in immune cell
265 activation, we assessed the level of TIGIT expression and found that while there was no difference
266 in TIGIT expression in the thymus, spleen, or MLN, there was increased expression on Tconv
267 (1.55-fold; p=0.0317) and CD8^{+} T cells (1.59-fold; p=0.0450), but unchanged on Tregs (including
268 early, normal, and ex-Treg subsets), in PLNs from *Cd226* gKO versus WT mice (**Supplemental**

269 **Figure 2**). This suggests that loss of CD226 coupled with increased TIGIT may contribute to the
270 diabetes protection previously observed in *Cd226* gKO NOD mice (17).
271

272 **Generation of *Cd226*$^{fl/fl}$ Treg-specific cKO NOD mice**

273 While the germline *Cd226* KO demonstrated a reduction of ex-Treg, an increase in early Tregs,
274 and an enrichment for TIGIT^{+} Tconv and CD8^{+} T cells in the disease-relevant inflammatory
275 environment of the PLN, it does not preclude the possibility that these observations could be
276 secondary to the diabetes-protected phenotype of the *Cd226* gKO, resulting from Treg-extrinsic
277 factors (17). To investigate the intrinsic role of CD226 on Tregs and how the loss of this signaling
278 might affect diabetes pathogenesis, we generated NOD mice expressing a *Cd226* cKO allele by
279 inserting loxP sequences flanking exon 2 of *Cd226* (*Cd226*$^{fl/fl}$). We then crossed these mice with
280 the NOD.*Foxp3*-GFP-Cre strain (20) to selectively reduce CD226 expression in Foxp3-expressing
281 Tregs (**Fig. 3A**). PCR amplification of the *Cd226*^{fl} allele in sorted CD4^{+}GFP^{+} Treg, CD4^{+}GFP^{-}
282 Tconv, and CD8^{+} T cells from *Cd226*$^{fl/fl}$.*Foxp3*-GFP-Cre$^{+/-}$ (Treg$^{\Delta Cd226}$) splenocytes showed a
283 truncated *Cd226* amplicon (381 base pairs) from Tregs compared to CD4^{+} Tconv and CD8^{+} T cells
284 (868 base pairs) (**Supplemental Figure 3**), confirming successful cKO. Expression of CD226 was
285 reduced on Tregs in a *Cd226*^{fl} allele-dose dependent manner (**Fig. 3B-C**). Inhibition of CD226
286 expression was strongly selective towards Tregs, as CD226 surface expression was maintained in
287 CD4^{+} Tconv and CD8^{+} T cells (**Fig. 3D-E**). Overall, these data validate the selectiveness of the
288 Treg$^{\Delta Cd226}$ strain, leading us to study the impacts of this genetic modification on diabetes
289 pathogenesis.
290

291 **Treg *Cd226* cKO reduced insulitis and diabetes incidence in female NOD mice**

292 To determine the effect of the selective deletion of CD226 on Tregs in the context of diabetes
293 pathogenesis in NOD mice, we performed insulitis scoring on hematoxylin and eosin (H&E)-
294 stained pancreas sections from age-matched pre-diabetic Treg$^{\Delta Cd226}$ and Treg^{WT} mice (**Fig. 4A-B**).
295 Insulitis scores were reduced in 12-week-old female Treg$^{\Delta Cd226}$ mice (p<0.0001) while insulitis
296 severity was comparable in 16-week-old male Treg$^{\Delta Cd226}$ and Treg^{WT} NODs (p=0.47, **Fig. 4C-D**).
297 In line with this, female Treg$^{\Delta Cd226}$ mice had reduced diabetes incidence (44.0%) as compared to
298 Treg^{WT} (66.7%; p=0.042) and *Cd226*$^{fl/fl}$.*Foxp3*$^{+/+}$ controls (75.0%; p=0.012). We did not observe
299 a significant difference in diabetes incidence between female Treg^{WT} and *Cd226*$^{fl/fl}$.*Foxp3*$^{+/+}$
300 control groups (p=0.5985). Interestingly, diabetes incidence in male mice was unchanged between
301 Treg$^{\Delta Cd226}$ and Treg^{WT} genotypes (p=0.3367, **Fig. 4E-F**). While we previously reported that *Cd226*
302 gKO led to decreased dacryoadenitis in male NOD mice (17), we did not observe a significant
303 difference in lacrimal gland focus scores of 16-week-old Treg^{WT} and Treg$^{\Delta Cd226}$ mice (p=0.1613;
304 **Supplemental Figure 4**). Thus, we chose to focus on female NOD mice in our further
305 characterization of the Treg$^{\Delta Cd226}$ strain.

306

307 **TIGIT surface expression is increased on Tregs in Treg$^{\Delta Cd226}$ mice**

308 To determine the basis of the protection observed in female Treg$^{\Delta Cd226}$ mice, we first performed *ex*
309 *vivo* phenotyping of spleen, PLN, and pancreas by flow cytometry (**Supplementary Figure 5A**).
310 We observed that bulk CD8$^+$ and CD4$^+$ T cell frequencies were unchanged in the spleen, PLN, and
311 pancreas of Treg$^{\Delta Cd226}$ and Treg^{WT} mice (**Supplementary Figure 5B-C**). Within the CD4$^+$
312 compartment, CD4$^+$Foxp3$^-$ Tconv and CD4$^+$Foxp3$^+$ Treg frequencies were similar between
313 Treg$^{\Delta Cd226}$ and Treg^{WT} NODs in all three tissues evaluated (**Supplementary Figure 5D-E**). Since

314 CD226 is upregulated in EM T cell subsets from WT NODs (**Figure 1**) (8, 14), we next examined
315 the frequencies of $CD44^{-}CD62L^{+}$ naïve and $CD44^{+}CD62L^{-}$ EM T cells and found that there was
316 no difference in naïve or EM $CD8^{+}$ T cells, $CD4^{+}$ Tconv and Tregs between $Treg^{\Delta Cd226}$ and $Treg^{WT}$
317 mice (**Supplementary Figure 6**). Furthermore, $Treg^{\Delta Cd226}$ and $Treg^{WT}$ mice showed no differences
318 in thymic Treg ($Foxp3^{+}Helios^{+}$ or $Foxp3^{+}Nrp1^{+}$) or peripheral Tregs ($Foxp3^{+}Helios^{-}$ or
319 $Foxp3^{+}Nrp1^{-}$) frequencies in the thymus, spleen, PLN, and pancreas (**Supplementary Figure 7**)
320 (24-27). Overall, this data suggests that the protection from diabetes provided by $Treg^{\Delta Cd226}$ was
321 not due to increased numbers of Tregs in the periphery and that Treg *Cd226* cKO did not lead to
322 any intrinsic changes in memory Treg formation or extrinsic changes in Tconv cells.

323 Due to the opposing roles of CD226 and TIGIT and the increased TIGIT on effector T cells
324 observed in *Cd226* gKO PLNs (**Supplementary Figure 2**), we next examined TIGIT geometric
325 mean fluorescence intensity (gMFI) in $Treg^{\Delta Cd226}$ mice. Interestingly, TIGIT surface expression
326 on Tregs was increased in the spleens (p=0.0002), PLNs (p=0.0002), and pancreas (p<0.0001) of
327 $Treg^{\Delta Cd226}$ mice (**Fig. 5A-B**). In contrast, there was increased TIGIT expression in $CD4^{+}$ Tconv in
328 the spleen (p=0.0461) and pancreas (p<0.0001), but not PLN (p=0.2501), of $Treg^{\Delta Cd226}$ mice (**Fig.
329 5C**). Furthermore, there was no change in TIGIT surface expression in $CD8^{+}$ T cells in the organs
330 examined (**Fig. 5D**). This suggests that increased TIGIT signaling in Tregs secondary to the loss
331 of CD226 may contribute to the delayed disease progression observed in female $Treg^{\Delta Cd226}$ NOD
332 mice.

333

334 **$Treg^{\Delta Cd226}$ effector T cells show reduced proliferation in response to *in vitro* stimulation**

335 To assess whether the lack of CD226 signaling on Tregs would affect T cell activation, we
336 performed short time-course stimulation studies to determine the magnitude of TCR and co-

337 stimulatory signaling via measurement of phosphorylated Akt (pAkt; pS473) and ribosomal
338 protein S6 (pS6; pS235/pS236) in splenocytes activated with plate-bound α-CD3ε/CD155-Fc. We
339 found that while there was no difference in pAkt gMFI of Treg$^{\Delta Cd226}$ and Treg^{WT} splenocytes (**Fig.**
340 **6A-C**), there was a decrease in pS6^{+} CD8^{+} T cells from Treg$^{\Delta Cd226}$ mice after 30 minutes of
341 stimulation (p=0.0304; **Fig. 6D-F**). This suggests that Treg *Cd226* cKO may result in a CD8^{+} T
342 cell-extrinsic mechanism of TCR signaling. We next stimulated splenocytes *in vitro* with α-
343 CD3ε/α-CD28 or α-CD3ε/CD155-Fc conditions and assessed the proliferation of T cell subsets
344 via dye dilution as measured by flow cytometry. In response to α-CD3ε/CD155-Fc, but not α-
345 CD3ε/α-CD28, proliferation was reduced in CD8^{+} (p=0.0030) and CD4^{+} T cells (p=0.0002) from
346 Treg$^{\Delta Cd226}$ compared to Treg^{WT} mice (**Fig. 6G-J**). Altogether, these findings suggest that reduced
347 CD8^{+} T cell proliferation, secondary to reduced S6 phosphorylation downstream of TCR signaling,
348 could be a key mechanism by which insulitis and diabetes incidence are inhibited in Treg$^{\Delta Cd226}$
349 mice.

350 **Discussion**

351 In this study, we determined that CD226 signaling in Tregs contributes to diabetes pathogenesis
352 in female NOD mice. In agreement with previous reports (21, 22), we found that stable EM Tregs
353 highly expressed CD226. Additionally, we found significantly higher CD226 expression in ex-
354 Tregs which has not been previously reported. Global *Cd226* deletion on the NOD background led
355 to decreased ex-Treg frequencies in the PLN, highlighting the notion that excess activation
356 provided by CD226 signaling may lead to Treg instability and the loss of Foxp3 expression. In
357 contrast, others have shown in a humanized mouse model of GVHD that murine Tregs deficient
358 in CD226 have greater TIGIT signaling and in turn, improved maintenance of Foxp3 expression
359 (16). Interestingly, *Cd226* gKO did not affect early Treg, normal Treg, or ex-Treg frequencies in
360 the thymus, spleen, or MLN, demonstrating that CD226 deletion did not impair central or
361 peripheral Treg development. This is in contrast with the defects observed in NOD.*Cd28* KO mice
362 in thymic Treg development and peripheral maintenance when the loss of CD28-B7 co-stimulation
363 resulted in decreased CD25 expression on Tregs and IL-2 production by Tconv (28-30). The
364 protection and reduced PLN ex-Tregs in *Cd226* gKO mice prompted us to interrogate the role of
365 CD226 on Treg function in NOD disease apart from the risk conferred through CD226 activity
366 within other immune cell subsets.

367 Generation of the NOD.$Cd226^{fl/fl}$ strain and crossing with the NOD.*Foxp3*-GFP-Cre strain
368 demonstrated Treg-selective *Cd226* cKO and decreased diabetes pathogenesis in female NOD
369 mice. Flow cytometric studies showed that naïve and EM Treg, $CD4^+$ Tconv, and $CD8^+$ T cell
370 frequencies were unaffected in $Treg^{\Delta Cd226}$ mice, suggesting there was no impairment of T cell
371 activation of Treg cKO mice. We also observed a significant increase in TIGIT surface expression
372 on Tregs in the spleen, PLN, and pancreas, along with increased TIGIT expression of $CD4^+$ Tconv

373 in the pancreas of Treg$^{\Delta Cd226}$ versus Treg^{WT} mice. Wang and colleagues observed a similar
374 phenotype, reporting that *Cd226*$^{-/-}$ C57BL/6 mice after inducing EAE showed increased CTLA-4
375 and TIGIT expression on Tregs in the central nervous system (31). We observed decreased pS6^{+}
376 in CD8^{+} T cells and proliferation of CD4^{+} and CD8^{+} T cells in response to *in vitro* α-CD3ε/CD155-
377 Fc stimulation of Treg$^{\Delta Cd226}$ versus Treg^{WT} splenocytes. We surmise that the inhibition of Teff
378 proliferation in Treg$^{\Delta Cd226}$ mice may be due to enhanced Treg suppression mediated through
379 increased TIGIT-CD155 interactions, which others have shown to increase IL-10 production by
380 CD4^{+} T cells and Tregs (32, 33) as well as dendritic cells (34). Decreased S6 phosphorylation,
381 which lies downstream of the Akt signaling cascade, corresponds with a previous report showing
382 that the *Cd226*$^{-/-}$ EAE mouse had decreased pAkt and pErk signaling in Tregs (31). This suggests
383 that CD226-deficient Tregs prevent diabetes pathogenesis by reducing effector T cell activation
384 and proliferation through increased IL-10 production mediated by increased TIGIT-CD155
385 interactions.

386 The delayed onset and reduced incidence of diabetes in genomic and Treg-conditional
387 *Cd226* KO NOD mice demonstrates the utility of the NOD model in studying interventions
388 modulating CD226/TIGIT signaling and how they may affect autoimmune T1D pathogenesis. The
389 interesting finding that there was no difference in insulitis or diabetes progression in male
390 Treg$^{\Delta Cd226}$ mice could be due to the inherently low disease incidence of WT male NOD mice (5%
391 in the current study) (35). Future studies may include crossing Treg-fate and *Cd226* cKO strains
392 to determine how CD226 activity in Tregs intrinsically affects their potential development into ex-
393 Tregs. Additionally, the NOD.*Cd226*$^{fl/fl}$ mice could readily be crossed with additional strains, such
394 as NOD.*Gzmb*-Cre and NOD.*Cd8*-Cre mice, to study effects of NK and CD8^{+} T cell-specific
395 *Cd226* cKO. The detailed mechanistic studies reported herein support strategies to block CD226

signaling, particularly on Tregs, to interrupt T1D progression. Hence, future studies are needed to evaluate therapeutics modulating this costimulatory pathway for the ability to delay or prevent autoimmune diabetes in the NOD pre-clinical model in support of future translation to clinical trials.

Acknowledgments

We would like to acknowledge Thinzar Myint, M.S. (University of Florida) for project coordination and support. We would also like to thank Kayla Nguyen and Jin-Ju Lee (University of Florida) for technical assistance with blood glucose monitoring. Treg-fate tracking NOD mice were a kind gift from Dr. Jeffrey Bluestone (University of California San Francisco).

Author Contributions

PT: Data curation, Formal analysis, Funding acquisition, Investigation, Methodology, Project administration, Validation, Visualization, Writing-original draft, Writing-review & editing

MEB: Investigation, Visualization, Writing-review & editing

LKS: Investigation, Writing-review & editing

JMA: Investigation, Writing-review & editing

W-IY: Investigation, Writing-review & editing

ALP: Writing-review & editing

MRS: Funding acquisition, Investigation, Methodology, Writing-review & editing

YGC: Investigation, Writing-review & editing

TMB: Conceptualization, Funding acquisition, Methodology, Resources, Supervision, Writing-review & editing

Funding

Project funding was provided by the National Institutes of Health (NIH; R01 DK106191 to TMB; F30 DK128945 to PT), the Helmsley Charitable Trust Foundation (2004-03813 to TMB), and Diabetes Research Connection (Project #45 to MRS).

Conflict of Interest Statement

The authors have declared that no relevant conflicts of interest exist.

427 **References**

428 1. Hafler JP, Maier LM, Cooper JD, Plagnol V, Hinks A, Simmonds MJ, et al. CD226
429 Gly307Ser association with multiple autoimmune diseases. Genes & Immunity. 2009;10(1):5-10.
430 2. Qiu Z-X, Zhang K, Qiu X-S, Zhou M, Li W-M. CD226 Gly307Ser association with
431 multiple autoimmune diseases: A meta-analysis. Human Immunology. 2013;74(2):249-55.
432 3. Zhang Z, Wu N, Lu Y, Davidson D, Colonna M, Veillette A. DNAM-1 controls NK cell
433 activation via an ITT-like motif. Journal of Experimental Medicine. 2015;212(12):2165-82.
434 4. Gilfillan S, Chan CJ, Cella M, Haynes NM, Rapaport AS, Boles KS, et al. DNAM-1
435 promotes activation of cytotoxic lymphocytes by nonprofessional antigen-presenting cells and
436 tumors. Journal of Experimental Medicine. 2008;205(13):2965-73.
437 5. Kojima H, Kanada H, Shimizu S, Kasama E, Shibuya K, Nakauchi H, et al. CD226
438 Mediates Platelet and Megakaryocytic Cell Adhesion to Vascular Endothelial Cells. Journal of
439 Biological Chemistry. 2003;278(38):36748-53.
440 6. Reymond N, Imbert A-M, Devilard E, Fabre SP, Chabannon C, Xerri L, et al. DNAM-1
441 and PVR Regulate Monocyte Migration through Endothelial Junctions. Journal of Experimental
442 Medicine. 2004;199(10):1331-41.
443 7. Vo AV, Takenaka E, Shibuya A, Shibuya K. Expression of DNAM-1 (CD226) on
444 inflammatory monocytes. Molecular Immunology. 2016;69:70-6.
445 8. Dardalhon V, Schubart AS, Reddy J, Meyers JH, Monney L, Sabatos CA, et al. CD226 Is
446 Specifically Expressed on the Surface of Th1 Cells and Regulates Their Expansion and Effector
447 Functions. The Journal of Immunology. 2005;175(3):1558-65.
448 9. Fourcade J, Sun Z, Chauvin J-M, Ka M, Davar D, Pagliano O, et al. CD226 opposes
449 TIGIT to disrupt Tregs in melanoma. JCI Insight. 2018;3(14).
450 10. Gaud G, Roncagalli R, Chaoui K, Bernard I, Familiades J, Colacios C, et al. The
451 costimulatory molecule CD226 signals through VAV1 to amplify TCR signals and promote IL-
452 17 production by CD4. Sci Signal. 2018;11(538).
453 11. Jacobsen LM, Newby BN, Perry DJ, Posgai AL, Haller MJ, Brusko TM. Immune
454 Mechanisms and Pathways Targeted in Type 1 Diabetes. Current Diabetes Reports. 2018;18(10).
455 12. Atkinson MA, Roep BO, Posgai A, Wheeler DCS, Peakman M. The challenge of
456 modulating β-cell autoimmunity in type 1 diabetes. The Lancet Diabetes & Endocrinology.
457 2019;7(1):52-64.
458 13. Mcclymont SA, Putnam AL, Lee MR, Esensten JH, Liu W, Hulme MA, et al. Plasticity
459 of Human Regulatory T Cells in Healthy Subjects and Patients with Type 1 Diabetes. The
460 Journal of Immunology. 2011;186(7):3918-26.
461 14. Fuhrman CA, Yeh W-I, Seay HR, Saikumar Lakshmi P, Chopra G, Zhang L, et al.
462 Divergent Phenotypes of Human Regulatory T Cells Expressing the Receptors TIGIT and
463 CD226. The Journal of Immunology. 2015;195(1):145-55.
464 15. Brown ME, Peters LD, Hanbali SR, Arnoletti JM, Sachs LK, Nguyen KQ, et al. Human
465 CD4+CD25+CD226- Tregs Demonstrate Increased Purity, Lineage Stability, and Suppressive
466 Capacity Versus CD4+CD25+CD127lo/- Tregs for Adoptive Cell Therapy. Frontiers in
467 Immunology. 2022;13.
468 16. Sato K, Yamashita-Kanemaru Y, Abe F, Murata R, Nakamura-Shinya Y, Kanemaru K, et
469 al. DNAM-1 regulates Foxp3 expression in regulatory T cells by interfering with TIGIT under
470 inflammatory conditions. Proceedings of the National Academy of Sciences.
471 2021;118(21):e2021309118.

17. Shapiro MR, Yeh W-I, Longfield JR, Gallagher J, Infante CM, Wellford S, et al. CD226 Deletion Reduces Type 1 Diabetes in the NOD Mouse by Impairing Thymocyte Development and Peripheral T Cell Activation. Frontiers in Immunology. 2020;11.
18. Wang N, Yi H, Fang L, Jin J, Ma Q, Shen Y, et al. CD226 Attenuates Treg Proliferation via Akt and Erk Signaling in an EAE Model. Frontiers in Immunology. 2020;11.
19. Zhang R, Zeng H, Zhang Y, Chen K, Zhang C, Song C, et al. CD226 ligation protects against EAE by promoting IL-10 expression via regulation of CD4+ T cell differentiation. Oncotarget. 2016;7(15):19251-64.
20. Zhou X, Bailey-Bucktrout SL, Jeker LT, Penaranda C, Martínez-Llordella M, Ashby M, et al. Instability of the transcription factor Foxp3 leads to the generation of pathogenic memory T cells in vivo. Nature Immunology. 2009;10(9):1000-7.
21. Monaco G, Lee B, Xu W, Mustafah S, Hwang YY, Carré C, et al. RNA-Seq Signatures Normalized by mRNA Abundance Allow Absolute Deconvolution of Human Immune Cell Types. Cell Reports. 2019;26(6):1627-40.e7.
22. Shapiro MR, Thirawatananond P, Peters L, Sharp RC, Ogundare S, Posgai AL, et al. De-coding genetic risk variants in type 1 diabetes. Immunology & Cell Biology. 2021;99(5):496-508.
23. Lucca LE, Axisa P-P, Singer ER, Nolan NM, Dominguez-Villar M, Hafler DA. TIGIT signaling restores suppressor function of Th1 Tregs. 2019.
24. Thornton AM, Korty PE, Tran DQ, Wohlfert EA, Murray PE, Belkaid Y, et al. Expression of Helios, an Ikaros Transcription Factor Family Member, Differentiates Thymic-Derived from Peripherally Induced Foxp3⁺ T Regulatory Cells. The Journal of Immunology. 2010;184(7):3433-41.
25. Yadav M, Louvet C, Davini D, Gardner JM, Martinez-Llordella M, Bailey-Bucktrout S, et al. Neuropilin-1 distinguishes natural and inducible regulatory T cells among regulatory T cell subsets in vivo. Journal of Experimental Medicine. 2012;209(10):1713-22.
26. Weiss JM, Bilate AM, Gobert M, Ding Y, Curotto De Lafaille MA, Parkhurst CN, et al. Neuropilin 1 is expressed on thymus-derived natural regulatory T cells, but not mucosa-generated induced Foxp3+ T reg cells. Journal of Experimental Medicine. 2012;209(10):1723-42.
27. Singh K, Hjort M, Thorvaldson L, Sandler S. Concomitant analysis of Helios and Neuropilin-1 as a marker to detect thymic derived regulatory T cells in naïve mice. Scientific Reports. 2015;5(1):7767.
28. Salomon B, Lenschow DJ, Rhee L, Ashourian N, Singh B, Sharpe A, et al. B7/CD28 Costimulation Is Essential for the Homeostasis of the CD4+CD25+ Immunoregulatory T Cells that Control Autoimmune Diabetes. Immunity. 2000;12(4):431-40.
29. Tang Q, Henriksen KJ, Boden EK, Tooley AJ, Ye J, Subudhi SK, et al. Cutting Edge: CD28 Controls Peripheral Homeostasis of CD4⁺CD25⁺ Regulatory T Cells. The Journal of Immunology. 2003;171(7):3348-52.
30. Tai X, Cowan M, Feigenbaum L, Singer A. CD28 costimulation of developing thymocytes induces Foxp3 expression and regulatory T cell differentiation independently of interleukin 2. Nature Immunology. 2005;6(2):152-62.
31. Wang N, Liang S, Jin J, Fang L, Ma Q, Wang X, et al. CD226 attenuates Treg suppressive capacity via CTLA-4 and TIGIT during EAE. Immunologic Research. 2019;67(6):486-96.

517 32. Joller N, Hafler JP, Brynedal B, Kassam N, Spoerl S, Levin SD, et al. Cutting Edge:
518 TIGIT Has T Cell-Intrinsic Inhibitory Functions. The Journal of Immunology.
519 2011;186(3):1338-42.
520 33. Joller N, Lozano E, Burkett R, Patrick, Patel B, Xiao S, Zhu C, et al. Treg Cells
521 Expressing the Coinhibitory Molecule TIGIT Selectively Inhibit Proinflammatory Th1 and Th17
522 Cell Responses. Immunity. 2014;40(4):569-81.
523 34. Yu X, Harden K, C Gonzalez L, Francesco M, Chiang E, Irving B, et al. The surface
524 protein TIGIT suppresses T cell activation by promoting the generation of mature
525 immunoregulatory dendritic cells. Nature Immunology. 2009;10(1):48-57.
526 35. Makino S, Kunimoto K, Muraoka Y, Mizushima Y, Katagiri K, Tochino Y. Breeding of a
527 Non-Obese, Diabetic Strain of Mice. Experimental Animals. 1980;29(1):1-13.
528 36. Xue S, Posgai A, Wasserfall C, Myhr C, Campbell-Thompson M, Mathews CE, et al.
529 Combination Therapy Reverses Hyperglycemia in NOD Mice With Established Type 1 Diabetes.
530 Diabetes. 2015;64(11):3873-84.
531 37. Barr JY, Wang X, Meyerholz DK, Lieberman SM. CD8 T cells contribute to lacrimal
532 gland pathology in the nonobese diabetic mouse model of Sjögren syndrome. Immunology &
533 Cell Biology. 2017;95(8):684-94.
534

535 **Figures**

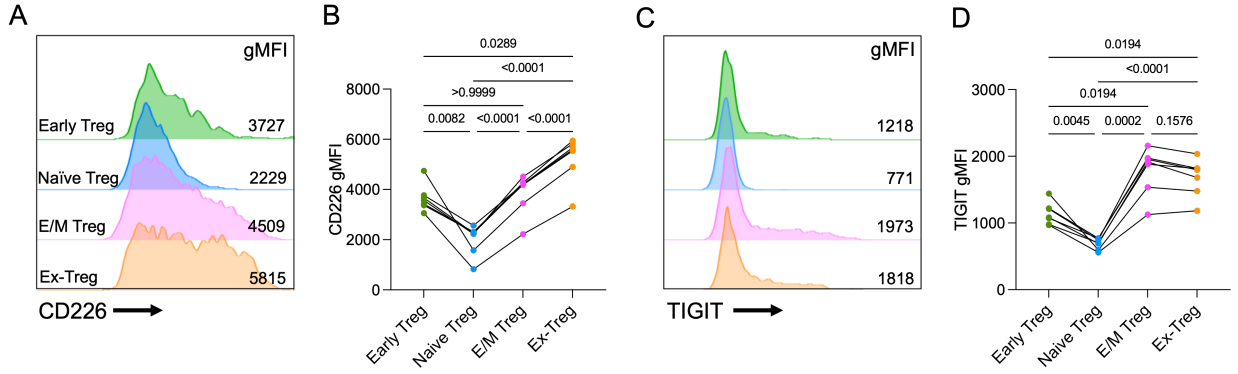

536

537 **Figure 1. CD226 and TIGIT expression levels in Tregs and ex-Tregs**. Splenocytes from pre-
538 diabetic 12-week-old male Treg-fate tracking NOD mice were assessed through spectral flow
539 cytometry. **(A)** Half-offset histograms and **(B)** quantification of CD226 geometric mean
540 fluorescence intensity (gMFI) on $GFP^{+}YFP^{-}$ early Treg, $GFP^{+}YFP^{+}CD44^{-}CD62L^{+}$ naïve Treg,
541 $GFP^{+}YFP^{+}CD44^{+}CD62L^{-}$ EM Treg, and $GFP^{-}YFP^{+}$ ex-Treg subsets. **(C)** Half-offset histograms
542 and **(D)** quantification of TIGIT gMFI. *P* values are displayed and were determined from repeated
543 measures one-way ANOVA with Bonferroni's multiple comparisons test (*n*=7).

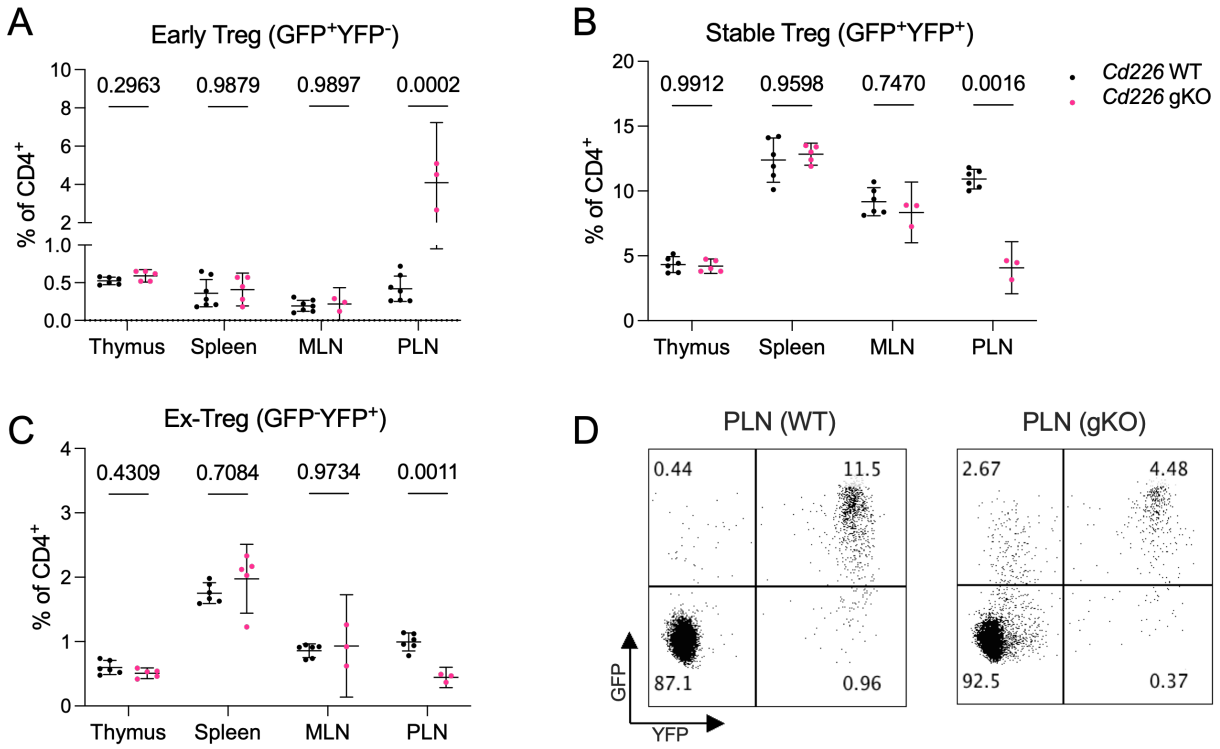

Figure 2. Decreased stable and ex-Tregs and increased pTreg in PLN of CD226 gKO NOD mice. (A) GFP$^+$YFP$^-$ "early" Tregs, **(B)** GFP$^+$YFP$^+$ stable Tregs, and **(C)** GFP$^-$YFP$^+$ ex-Tregs were quantified from thymus, spleen, mesenteric LN (MLN) and PLN from 12-week-old pre-diabetic male Treg-fate reporter mice with *Cd226* WT (n=7) or global knockout (gKO; n=5) alleles (plotted as a % of CD4$^+$ T cells following singlet, live, CD3ε$^+$ gating; analyzed using multiple t-tests with Sidak-Bonferroni multiple comparisons correction). **(D)** Representative flow cytometry from PLN of *Cd226* WT and gKO mice.

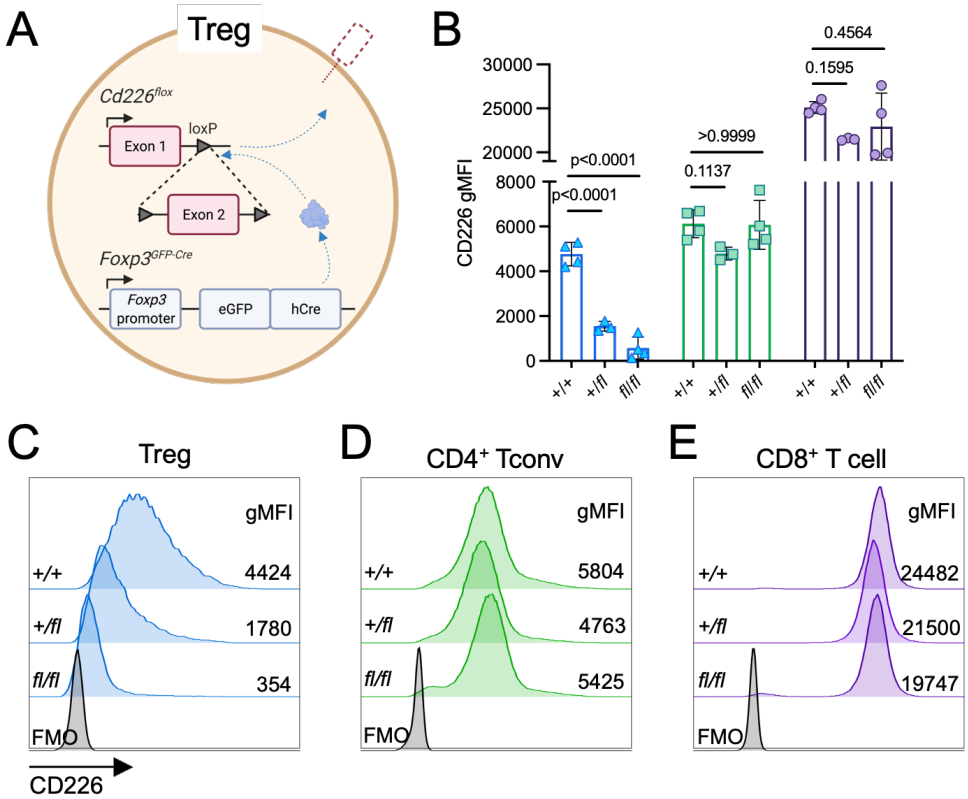

552

553 **Figure 3. CD226 gMFI is selectively reduced in Treg cKO NOD mice. (A)** Schematic of loxP
554 insertions flanking exon 2 (*fl*) of *Cd226* and excision in Tregs of Treg$^{\Delta Cd226}$ mice. **(B)** Scatter plot
555 showing CD226 gMFI and **(C-E)** representative histograms of CD4^{+}GFP^{+} Tregs (blue), CD4^{+}GFP^{-}
556 Tconv (green), and CD8^{+} T cells (purple) of 12-week-old pre-diabetic female *Cd226* +/+ (*n*=4),
557 +/fl (*n*=3), and fl/fl (*n*=3) mice versus fluorescence minus one (FMO) control. Analyzed with one-
558 way ANOVA with Bonferroni's multiple comparisons test.

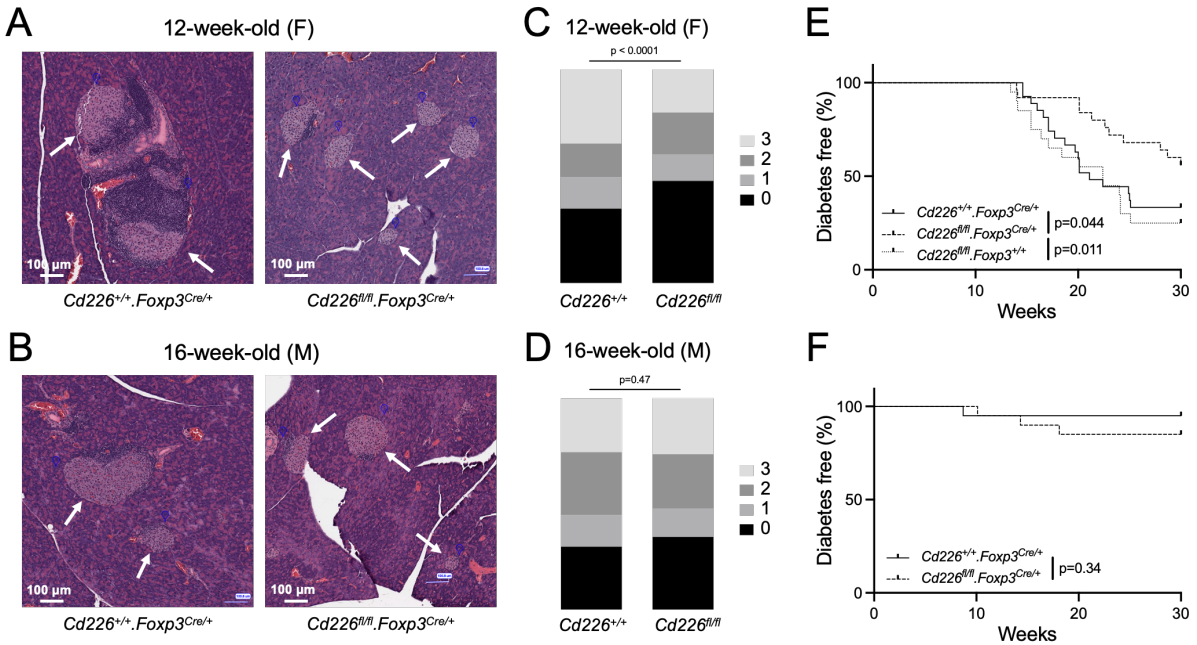

Figure 4. Treg *Cd226* cKO reduces insulitis and diabetes incidence in female NOD mice. (A-B) Representative H&E-stained pancreas sections with white arrows denoting islets of Langerhans and **(C-D)** stacked bar graphs depicting insulitis scores from 12-week-old female and 16-week-old male $Cd226^{+/+}.Foxp3^{Cre/+}$ (female, n=8 mice and 512 islets; male, n=5 mice and 252 islets) and $Cd226^{fl/fl}.Foxp3^{Cre/+}$ (female, n=8 mice and 443 islets; male, n=3 mice and 262 islets) NOD mice. Statistical analysis performed with Chi-square test. **(E-F)** Diabetes incidence curves from **(E)** female and **(F)** male NOD mice. Female N = $Cd226^{+/+}.Foxp3^{Cre/+}$, 27; $Cd226^{fl/fl}.Foxp3^{Cre/+}$, 20; $Cd226^{fl/fl}.Foxp3^{+/+}$, 20. Male N = $Cd226^{+/+}.Foxp3^{Cre/+}$, 20; $Cd226^{fl/fl}.Foxp3^{Cre/+}$, 20. Analyzed with Log-rank (Mantel-Cox) test.

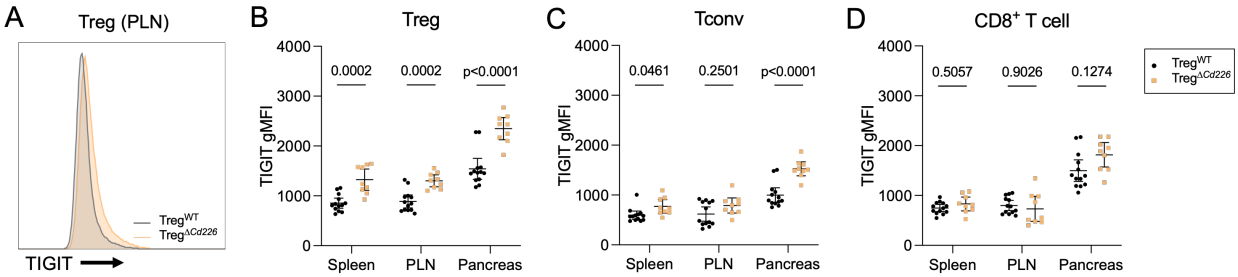

Figure 5. Treg$^{\Delta Cd226}$ mice show increased TIGIT expression compared to Treg^{WT} mice. (A) Overlaid histograms of TIGIT surface expression on Tregs in the PLN showing Treg^{WT} in black and Treg$^{\Delta Cd226}$ in orange. Quantification of TIGIT gMFI of **(B)** Tregs, **(C)** CD4^{+} Tconv, and **(D)** CD8^{+} T cells. Statistical analysis was performed with multiple t-tests with Sidak-Bonferroni multiple comparisons correction.

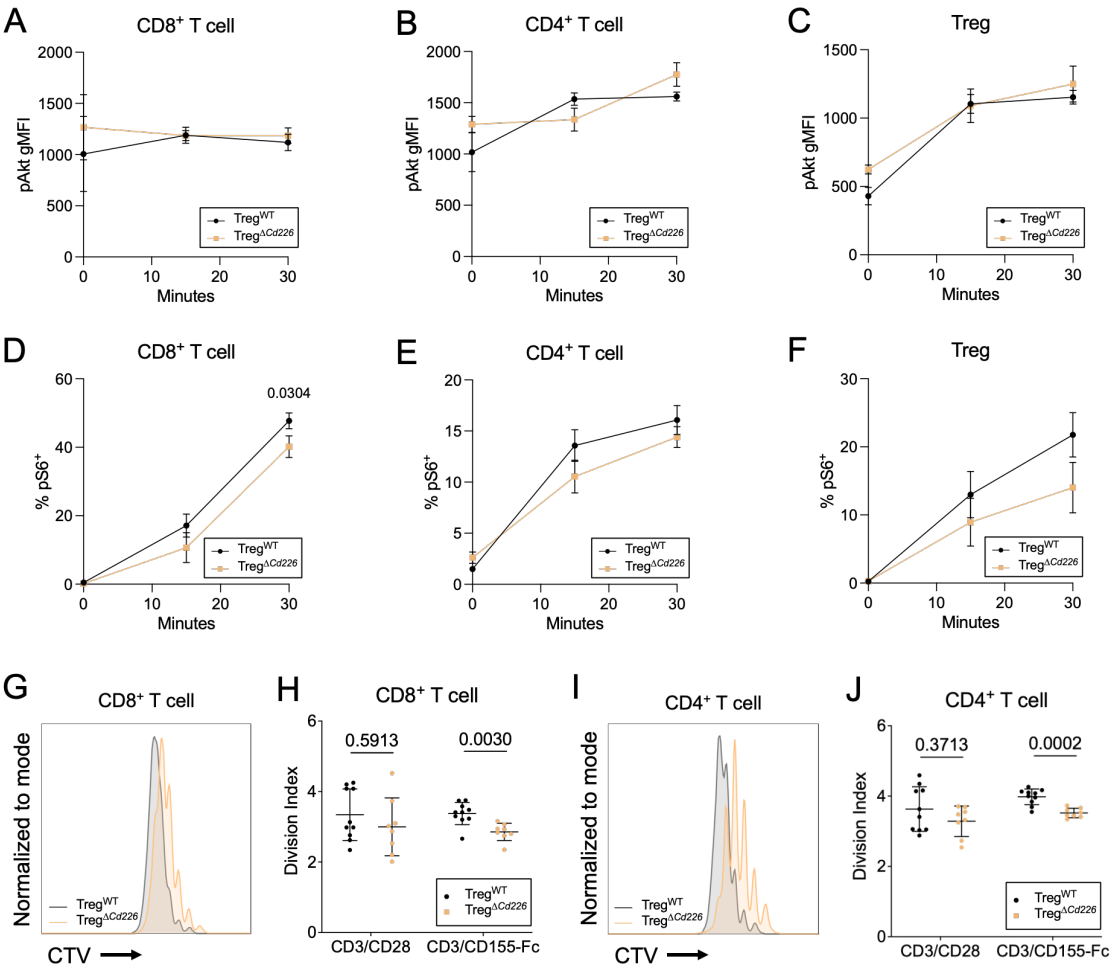

575

576 **Figure 6. Treg$^{\Delta Cd226}$ splenocytes have reduced proliferation in response to α-CD3ε/CD155-Fc**
577 **stimulus.** Quantification of **(A-C)** phospho-Akt (pAkt) gMFI and **(D-F)** phospho-S6^{+} (pS6)
578 ribonuclear protein in CD8^{+} T cells, CD4^{+} T cells, and Treg from Treg^{WT} (black) and Treg$^{\Delta Cd226}$
579 (orange) splenocytes (n=4) after stimulation with plate-bound α-CD3ε/CD155-Fc. Statistical
580 analyses were performed with 2-way ANOVA with Sidak multiple comparisons correction. **(G-J)**
581 Overlaid histograms showing CellTrace Violet dye dilution and division indices of CD8^{+} **(G** and
582 **H)** and CD4^{+} T cells **(I** and **J)** from 12-week-old female Treg^{WT} (black; n=10) and Treg$^{\Delta Cd226}$
583 (orange; n=7) splenocytes after four days of stimulation with plate-bound α-CD3ε/α-CD28 or
584 plate-bound α-CD3ε/CD155-Fc. Analyzed with multiple t-tests with Sidak-Bonferroni multiple
585 testing correction.